

# Real space operators for Stokes $Q$ & $U$ to scalars $E$ & $B$ translation

**Aditya Rotti and Kevin Huffenberger**

Department of Physics, Florida State University, Keen Physics Building, 77 Chieftan Way, Tallahassee, Florida, U.S.A.

E-mail: [adityarotti@gmail.com](mailto:adityarotti@gmail.com), [khuffenberger@fsu.edu](mailto:khuffenberger@fsu.edu)

**Abstract.** We derive fully sky real space operators to translate Stokes  $Q$  &  $U$  parameters to scalars  $E$  &  $B$  and vice versa. We explicitly show that these local real space operator are fully characterized by the spin-0  $Y_{\ell 2}$  spherical harmonic functions. These real space operators make transparent the association of radial and tangential patterns of polarization with the  $E$  modes and that of the clockwise and anti-clockwise pinwheel patterns of polarization with  $B$ -modes. We cast the standard CMB polarization analysis operators in a matrix-vector notation which elucidate these derivations. Using this new notation also allows us to derive real space operators which decompose the measured Stokes parameters into those corresponding to  $E$ -modes and  $B$ -modes respectively, without ever evaluating the scalar fields themselves. We use these analytical derivations us to quantify the non-local nature of the relation between the two representations of the polarization field. We present a prescription for generalizing these operators, which allow the non-local behavior of these operators to be a tunable parameter. We derive constraints on these generalized operators to ensure reliable recovery of the standard  $E$  and  $B$  fields and the corresponding power spectra. This is part 1 of a series of papers where we have derived the real space operators. In the following papers we will explore some of their applications.  $\Rightarrow$  Needs better blending.

---

## Contents

<b>1</b>	<b>Introduction</b>	<b>3</b>
<b>2</b>	<b>E/B description of CMB polarization</b>	<b>4</b>
2.1	Polarization primer	4
2.2	Matrix notation	5
<b>3</b>	<b>Real space operators</b>	<b>6</b>
3.1	Evaluating E & B fields from measured Stokes parameters Q & U	6
3.2	Evaluating Stokes parameters Q & U fields from E & B fields	8
3.3	Decomposing Q & U Stokes parameters into those corresponding to E & B modes respectively	9
3.4	Visualizing the convolution kernels	12
3.5	Quantifying the non-locality of E & B modes	14
<b>4</b>	<b>Generalized operators</b>	<b>17</b>
4.1	Recovering the default E and B mode spectra	19
<b>5</b>	<b>Discussion</b>	<b>21</b>
<b>6</b>	<b>Appendix</b>	<b>23</b>
6.1	Mathematical properties of spin spherical harmonics	23
6.2	The flat sky limit	23

---

**Some comments, questions and ideas that occurred to me while writing the draft:**

1. Using these local convolution can one now understand the E to B leakage occurring due to masking ?
2. Healpix has rings at constant latitude. So the real space convolution is only perfect for pixels near the pole ? What happens when you consider pixels around any arbitrary pixel on a Healpix map, they are probably not arranged in rings. Maybe for this reason working with upgraded map works and finer pixels allow for a better approximation of rings around arbitrary pixels ??
3. The Zaldariagga radial function  $1/\theta^2$  cannot be correct, since it does not vanish at  $\beta = \pi$ , while it is defined to be zero at  $\beta = 0$ . I guess since its in the flat sky limit, the  $\beta = \pi$  issue is not relevant.

**To do list:**

1. Check whether the local Healpix works for primordial B-mode spectrum.
2. Check the generation of local kernels by using a an effective beam in harmonic space. pl2 transformed
3. How do the coefficients of expansion for some radially compact kernel, derived from pl2 transforms differ from that of a pl0 transform ?

## 1 Introduction

In this work we follow the convention in which bar-ed variables correspond to those in real space, while the tilde-ed variables correspond to those in harmonic space [1].

This paper is organized in the following manner: In Sec. 2 we present a primer on the description of CMB polarization on the sphere and introduce the matrix notation which provides a more concise description of the same. In Sec. 3 we introduce the necessary tools and discuss the derivations of the real space operators. In Sec. 3.4 we evaluate the real space operators and present visualizations of these functions. Here we also discuss the locality of the real space E & B operators. In Sec. ?? we implement these operators to evaluate E & B maps from the Stokes parameters Q & U and compare these maps and their spectra from those derived using Healpix. We conclude with a discussion and the scope of this new method of analyzing CMB polarization in Sec. 5.

## 2 E/B description of CMB polarization

### 2.1 Polarization primer

The CMB polarization is measured in terms of Stokes Q and U parameters. These measurements can be combined to form the complex spin 2 polarization field as follows,

$$\begin{aligned}\pm_2 \bar{X}(\hat{n}) &= Q(\hat{n}) \pm iU(\hat{n}) \\ &= \sum_{\ell m} \pm_2 \tilde{X}_{\ell m} \pm_2 Y_{\ell m}(\hat{n}).\end{aligned}\quad (2.1)$$

Since these measured quantities depend on the local coordinate system, it is cumbersome to work with them. To overcome this, one describes the CMB polarization field in terms of a scalar field denoted by  $E(\hat{n})$  and a pseudo scalar field  $B(\hat{n})$  [2]. These scalar fields are related to the spin-2 polarization field  $\pm_2 X(\hat{n})$  via the following relations,

$$\mathcal{E}(\hat{n}) = -\frac{1}{2} [\bar{\partial}_{+2}^2 \bar{X}(\hat{n}) + \bar{\partial}_{-2}^2 \bar{X}(\hat{n})] ; \mathcal{B}(\hat{n}) = -\frac{1}{2i} [\bar{\partial}_{+2}^2 X(\hat{n}) - \bar{\partial}_{-2}^2 X(\hat{n})], \quad (2.2)$$

where  $\bar{\partial}$  and  $\bar{\partial}$  denote the spin raising and lowering operators respectively. These  $E$  and  $B$  fields are spin-0 fields similar to the temperature anisotropies and hence their value are independent of the coordinate system definitions (except that the B-modes have an odd parity, meaning that they change sign under reflection  $\hat{n} \rightarrow -\hat{n}$ ). The spin raising and lowering operators have the following properties [3],

$$\bar{\partial}_s Y_{lm}(\hat{n}) = \sqrt{(\ell-s)(\ell+s+1)} {}_{s+1} Y_{lm}(\hat{n}), \quad (2.3a)$$

$$\bar{\partial}_s Y_{lm}(\hat{n}) = -\sqrt{(\ell+s)(\ell-s+1)} {}_{s-1} Y_{lm}(\hat{n}), \quad (2.3b)$$

where  ${}_s Y_{lm}(\hat{n})$  denote the spin-s spherical harmonics.

Using Eq. (2.2) and the properties of the spin raising and lowering operators given in Eq. (2.3a) it can be shown that the scalar fields  $\mathcal{E}/\mathcal{B}$  are defined via the following set of equations,

$$\mathcal{E}(\hat{n}) = \sum_{\ell m} a_{\ell m}^E \sqrt{\frac{(\ell+2)!}{(\ell-2)!}} Y_{\ell m}(\hat{n}) ; \mathcal{B}(\hat{n}) = \sum_{\ell m} a_{\ell m}^B \sqrt{\frac{(\ell+2)!}{(\ell-2)!}} Y_{\ell m}(\hat{n}), \quad (2.4)$$

where the harmonic coefficients of  $\mathcal{E}/\mathcal{B}$  fields are related to the harmonic coefficients of the spin-2 polarization field via the following equations,

$$a_{\ell m}^E = -\frac{1}{2} [{}_{+2} \tilde{X}_{\ell m} + {}_{-2} \tilde{X}_{\ell m}] ; a_{\ell m}^B = -\frac{1}{2i} [{}_{+2} \tilde{X}_{\ell m} - {}_{-2} \tilde{X}_{\ell m}] \quad (2.5)$$

In the remainder of this article, we will work with the scalar  $E$  and pseudo scalar  $B$  fields as defined by the following expressions,

$$E(\hat{n}) = \sum_{\ell m} a_{\ell m}^E Y_{\ell m}(\hat{n}) ; B(\hat{n}) = \sum_{\ell m} a_{\ell m}^B Y_{\ell m}(\hat{n}). \quad (2.6)$$

Note that the  $[E, B]$  fields are merely filtered versions of the fields  $[\mathcal{E}, \mathcal{B}]$ , as their spherical harmonic coefficients of expansion differ by the factor of  $\sqrt{\frac{(\ell+2)!}{(\ell-2)!}}$ .

## 2.2 Matrix notation

In this section we cast the relation introduced in Sec. 2.1 in matrix notation<sup>1</sup>. This representation will make transparent the derivation of the real space operators we discuss in the following sections. We adopt a convention in which real space quantities are denoted by bar-ed variable while those in harmonic space are denoted by tilde-ed variables.

We begin by introducing the matrices encoding the spin spherical harmonic basis vectors,

$${}_{|s|}\mathcal{Y} = \begin{bmatrix} {}^{+s}Y & 0 \\ 0 & {}^{-s}Y \end{bmatrix}_{2N_{\text{pix}} \times 2N_{\text{alms}}}, \quad (2.7)$$

where  $s$  denotes the spin of the basis functions. For this work we will only be working with cases  $s \in [0, 2]$ . In this notation, each column can be mapped to a specific harmonic basis function marked by the pair of indices:  $(\ell, m)$  and each row maps to a specific position on the sphere. Note that this matrix is in general not a square matrix. The number of rows is determined by the scheme used to discretely represent the sphere and the number of columns is set by the number of basis functions of interest (often determined by the band limit).

We now define the different polarization data vectors and their representation in real and harmonic space as follows,

$$\bar{S} = \begin{bmatrix} E \\ B \end{bmatrix}_{2N_{\text{pix}} \times 1} ; \quad \bar{X} = \begin{bmatrix} {}^{+2}X \\ {}^{-2}X \end{bmatrix}_{2N_{\text{pix}} \times 1} ; \quad \bar{P} = \begin{bmatrix} Q \\ U \end{bmatrix}_{2N_{\text{pix}} \times 1}, \quad (2.8a)$$

$$\tilde{S} = \begin{bmatrix} a^E \\ a^B \end{bmatrix}_{2N_{\text{alms}} \times 1} ; \quad \tilde{X} = \begin{bmatrix} {}^{+2}\tilde{X} \\ {}^{-2}\tilde{X} \end{bmatrix}_{2N_{\text{alms}} \times 1}. \quad (2.8b)$$

The different symbols have the same meaning as that discussed in Sec. 2.1, except that the subscript  $\ell_m$  for the spherical harmonic coefficients of expansion is suppressed if favor of cleaner notation.

Next we define the operators which govern the transformations between different representations of the polarization field as follows,

$$\bar{T} = \begin{bmatrix} 1 & i\mathbb{1} \\ \mathbb{1} & -i\mathbb{1} \end{bmatrix}_{2N_{\text{pix}} \times 2N_{\text{pix}}} ; \quad \bar{T}^{-1} = \frac{1}{2}\bar{T}^\dagger, \quad (2.9a)$$

$$\tilde{T} = -\begin{bmatrix} 1 & i\mathbb{1} \\ \mathbb{1} & -i\mathbb{1} \end{bmatrix}_{2N_{\text{alms}} \times 2N_{\text{alms}}} ; \quad \tilde{T}^{-1} = \frac{1}{2}\tilde{T}^\dagger, \quad (2.9b)$$

where we have chosen the sign conventions so as to match those used in Healpix. Using the data vectors and the matrix operators defined above we can now express, in compact notation, the forward and inverse relations between different representations of the polarization data vectors as follows,

$$\bar{X} = \bar{T} * \bar{P} ; \quad \bar{P} = \frac{1}{2}\bar{T}^\dagger * \bar{X}, \quad (2.10a)$$

$$\bar{X} = {}_2\mathcal{Y} * \tilde{X} ; \quad \tilde{X} = {}_2\mathcal{Y}^\dagger * \bar{X}, \quad (2.10b)$$

$$\tilde{X} = \tilde{T} * \tilde{S} ; \quad \tilde{S} = \frac{1}{2}\tilde{T}^\dagger * \tilde{X}. \quad (2.10c)$$

$$\bar{S} = {}_0\mathcal{Y} * \tilde{S} ; \quad \tilde{S} = {}_0\mathcal{Y}^\dagger * \bar{S}. \quad (2.10d)$$

---

<sup>1</sup>While we work with the matrix and vector sizes given in terms of some pixelization parameter  $N_{\text{pix}}$ , all the relations are equally valid in the continuum limit attained by allowing  $N_{\text{pix}} \rightarrow \infty$

Next we introduce the harmonic space operators, which project the harmonic space data vector to E or B subspace,

$$\tilde{O}_E = \begin{bmatrix} 1 & 0 \\ 0 & 0 \end{bmatrix}_{2N_{\text{alms}} \times 2N_{\text{alms}}} ; \quad \tilde{S}_E = \tilde{O}_E * \tilde{S}, \quad (2.11a)$$

$$\tilde{O}_B = \begin{bmatrix} 0 & 0 \\ 0 & 1 \end{bmatrix}_{2N_{\text{alms}} \times 2N_{\text{alms}}} ; \quad \tilde{S}_B = \tilde{O}_B * \tilde{S} \quad (2.11b)$$

Note that these harmonic space matrices are idempotent, orthogonal to each other and their sum is an identity matrix as can be explicitly seen via the following relations,

$$\tilde{O}_E * \tilde{O}_E = \tilde{O}_E ; \quad \tilde{O}_B * \tilde{O}_B = \tilde{O}_B, \quad (2.12a)$$

$$\tilde{O}_E * \tilde{O}_B = 0, \quad (2.12b)$$

$$\tilde{O}_E + \tilde{O}_B = \mathbb{1}. \quad (2.12c)$$

Note that the above relations for these harmonic space operators are exactly valid. In the following sections we aim to derive the real space analogues of these harmonic space operators.

### 3 Real space operators

In this section we derive the real space operators which translate the Stokes vector  $\bar{P}$  to the vector of scalars  $\bar{S}$  and vice versa. We also derive real space operators for direct decomposition of the Stokes vector  $\bar{P}$  in to a vector  $\bar{P}_E$  that correspond to E-modes and another vector  $\bar{P}_B$  that corresponds to the B-modes of polarization, such that  $\bar{P} = \bar{P}_E + \bar{P}_B$  (without ever evaluating the E & B fields or their spherical harmonics). For carrying out these derivations we extensively use the matrix notation introduced in Sec. 2.2.

#### 3.1 Evaluating E & B fields from measured Stokes parameters Q & U

In Sec. 2.1 we described how the scalar fields E & B are derived from the Stokes parameters Q & U. To reiterate, this process involved taking the spin harmonic transform of the complex spin-2 field ( $\pm_2 \bar{X}$ ), taking linear combinations of the resultant coefficients of expansion ( $\pm_2 \tilde{X}_{\ell m}$ ) and evaluating the forward spin-0 transform to derive the scalar E & B fields. Here we derive the real space convolution kernels on the sphere which can be used to directly evaluate the scalar E & B fields on the sphere. We use the relations given in Eq. (2.10), to write down an equation relating the real space vector of scalars  $\bar{S}$  to the polarization vector  $\bar{P}$  as given below,

$$\bar{S} = {}_0\mathcal{Y} * \tilde{T}^{-1} * {}_2\mathcal{Y}^\dagger * \bar{T} * \bar{P} = \frac{1}{2} {}_0\mathcal{Y} * \tilde{T}^\dagger * {}_2\mathcal{Y}^\dagger * \bar{T} * \bar{P}, \quad (3.1a)$$

$$= \bar{O} * \bar{P}. \quad (3.1b)$$

The explicit form of the real space operator  $\bar{O}$  can be derived by contracting over all the matrix operators. This procedure of contracting over the operators is explicitly worked out in the following set of equations,

$$\bar{O} = \frac{1}{2} {}_0\mathcal{Y} * \tilde{T}^\dagger * {}_2\mathcal{Y}^\dagger * \bar{T}, \quad (3.2a)$$

$$= -0.5 \begin{bmatrix} {}_0Y_i & 0 \\ 0 & {}_0Y_i \end{bmatrix} \begin{bmatrix} \mathbb{1} & \mathbb{1} \\ -i\mathbb{1} & i\mathbb{1} \end{bmatrix} \begin{bmatrix} {}^{+2}Y_j^{T*} & 0 \\ 0 & {}^{-2}Y_j^{T*} \end{bmatrix} \begin{bmatrix} \mathbb{1} & i\mathbb{1} \\ \mathbb{1} & -i\mathbb{1} \end{bmatrix}, \quad (3.2b)$$

$$= -0.5 \begin{bmatrix} \sum({}_0Y_i {}^{+2}Y_j^{T*} + {}_0Y_i {}^{-2}Y_j^{T*}) & i\sum({}_0Y_i {}^{+2}Y_j^{T*} - {}_0Y_i {}^{-2}Y_j^{T*}) \\ -i\sum({}_0Y_i {}^{+2}Y_j^{T*} - {}_0Y_i {}^{-2}Y_j^{T*}) & \sum({}_0Y_i {}^{+2}Y_j^{T*} + {}_0Y_i {}^{-2}Y_j^{T*}) \end{bmatrix}, \quad (3.2c)$$

where the symbol  ${}_0Y_i$  is used to denote the sub-matrix  ${}_0Y_{\hat{n}_i \times \ell m} \equiv {}_0Y_{\ell m}(\hat{n}_i)$ , the symbol  ${}_{\pm 2}Y_j^{T*}$  is used to denote the matrix  ${}_{\pm 2}Y_{\ell m \times \hat{n}_j}^* \equiv {}_{\pm 2}Y_{\ell m}^*(\hat{n}_j)$  and the summation is over the multipole indices  $\ell, m$ . Using the conjugation properties of the spin spherical harmonic functions it can be shown that the following relation holds true,

$$\left[ \sum_{\ell m} {}_0Y_{\ell m}(\hat{n}_i) {}_{+2}Y_{\ell m}^*(\hat{n}_j) \right]^* = \sum_{\ell m} {}_0Y_{\ell m}(\hat{n}_i) {}_{-2}Y_{\ell m}^*(\hat{n}_j). \quad (3.3)$$

where the terms on either side of the equation are those that appear in Eq. (3.2c). Therefore the different parts of the real space operator  $\bar{O}$  are completely specified in terms of the complex function,

$$\begin{aligned} \mathcal{M}(\hat{n}_i, \hat{n}_j) &= \mathcal{M}_r + i\mathcal{M}_i, \\ &= \sum_{\ell m} {}_0Y_{\ell m}^*(\hat{n}_i) {}_2Y_{\ell m}(\hat{n}_j) = \sum_{\ell} \sqrt{\frac{2\ell+1}{4\pi}} {}_0Y_{\ell 2}(\beta_{ij}, \alpha_{ij}), \end{aligned} \quad (3.4a)$$

$$= \left[ \cos(2\alpha_{ij}) + i \sin(2\alpha_{ij}) \right] \sum_{\ell=\ell_{\min}}^{\ell_{\max}} \frac{2\ell+1}{4\pi} \sqrt{\frac{(\ell-2)!}{(\ell+2)!}} P_{\ell 2}(\cos \beta_{ij}), \quad (3.4b)$$

$$= \left[ \cos(2\alpha_{ij}) + i \sin(2\alpha_{ij}) \right] f(\beta_{ij}, \ell_{\min}, \ell_{\max}), \quad (3.4c)$$

where we have used the property of summation over spin spherical harmonics (see Eq. (6.1)) listed in Appendix 6.1. On simplifying Eq. (3.2c), the local convolution kernel can be cast in this simple form,

$$\bar{O} = - \begin{bmatrix} \mathcal{M}_r & \mathcal{M}_i \\ -\mathcal{M}_i & \mathcal{M}_r \end{bmatrix}_{2N_{\text{pix}} \times 2N_{\text{pix}}} = -f(\beta_{ij}, \ell_{\min}, \ell_{\max}) \begin{bmatrix} \cos(2\alpha_{ij}) & \sin(2\alpha_{ij}) \\ -\sin(2\alpha_{ij}) & \cos(2\alpha_{ij}) \end{bmatrix}, \quad (3.5)$$

where indices i,j map to the location  $\hat{n}_i$  and  $\hat{n}_j$  on the sphere. A similar equation for real space E & B operators was derived in [1], however those results were derived for the flat sky case and did not explicitly derive the radial kernel.  $\Rightarrow$  A discussion on this should be in the conclusions.

The scalar fields E & B can now be directly derived from the measured Stokes Q & U parameters by evaluating the following convolution,

$$\begin{bmatrix} E_i \\ B_i \end{bmatrix} = -\Delta\Omega \sum_{j=1}^{N_{\text{pix}}} f(\beta_{ij}, \ell_{\min}, \ell_{\max}) \begin{bmatrix} \cos(2\alpha_{ij}) & \sin(2\alpha_{ij}) \\ -\sin(2\alpha_{ij}) & \cos(2\alpha_{ij}) \end{bmatrix} \begin{bmatrix} Q_j \\ U_j \end{bmatrix}, \quad (3.6)$$

where  $\Delta\Omega$  denotes the pixel area and all the symbols have their usual meaning. The above equation can be expressed more concisely as follows,

$$[E + iB](\hat{n}_0) = -\Delta\Omega \sum_{j=1}^{N_{\text{pix}}} \left( \sum_{\ell=\ell_{\min}}^{\ell_{\max}} \frac{2\ell+1}{4\pi} \sqrt{\frac{(\ell-2)!}{(\ell+2)!}} P_{\ell 2}^2(\beta_{0j}) \right) \left( e^{-i2\alpha_{0j}} {}_{+2}X(\hat{n}_j) \right), \quad (3.7a)$$

$$= - \left( \left[ \sum_{\ell=\ell_{\min}}^{\ell_{\max}} \sqrt{\frac{2\ell+1}{4\pi}} Y_{\ell 2}^* \right] \circ {}_{+2}X \right) = - \left\{ \mathcal{M}^* \circ {}_{+2}X \right\}(\hat{n}_0), \quad (3.7b)$$

where  $\circ$  denotes a convolution and the spherical harmonic functions denote the rotated functions such that the pole of the function coincides with the direction  $\hat{n}_0$  and the reference zero for the azimuthal angle is the local longitude  $\phi_0$ . We know that the spin of product of functions with different spins is given by:  $s_1 f_{s_2} g = s_1 + s_2 h$ . Since  $[Q + iU]$  is a field with spin +2 and the function  $\exp(-i2\alpha)$  is a field with spin -2, the resultant field formed by the product of these two function has spin-0. This makes intuitive, the construction of the spin-0 E and B modes of polarization. Note that the coordinate dependence of the Stokes parameters cannot be integrated out at the location  $\hat{n}_0$  where the scalar fields are to be evaluated since the azimuthal angle becomes ill-defined. This issue is averted by the fact that the radial function is formed by taking weighted linear combinations of  $P_\ell^2$  Legendre polynomials which have vanishing contribution ( $P_\ell^2(\beta) \propto \sin^2 \beta$ ) as  $\beta \rightarrow 0, \pi$ . **Also note that the E-modes are constructed by product of functions ( $U \sin 2\alpha, Q \cos 2\alpha$ ) which have the same parity and hence have even parity while the B-modes are constructed by multiplying functions ( $Q \sin 2\alpha, U \cos 2\alpha$ ) of opposite parity and hence have an odd parity.**

Note that this kernel does not depend on the Euler angle  $\gamma \Rightarrow$  Why is that and how do you understand this? . This local convolution kernel has a part which depends only on the Euler angle  $\alpha$  which has no multipole dependence. The remaining part of the kernel is specified by the function  $f(\beta, \ell_{\min}, \ell_{\max})$  which depends only on the Euler angle  $\beta$  and completely incorporates the multipole  $\ell$  dependence of the kernel. We will refer to  $f(\beta, \ell_{\min}, \ell_{\max})$  as the radial part of the kernel since it only depends on the angular distance between different locations. Its the radial part of the kernel that completely determines the locality of this operator.

The azimuthal operations do not depend on the choice of basis functions, and can be argued as a requirement for constructing spin-0 fields by operating on spin-2 fields. The radial kernel however is determined by the choice of the basis functions. Motivated by this observation, one can now think of working with alternate basis functions which have different radial fall off.  $\Rightarrow$  This is generally true for all the local kernels. So shift this line to the section where we explore different radial functions.

### 3.2 Evaluating Stokes parameters Q & U fields from E & B fields

The real space operator which translates E & B fields to Stokes parameters Q & U is derived using a similar procedure. The inverse operator is given by the following expression,

$$\bar{P} = \bar{T}^{-1} * {}_2\mathcal{Y} * \tilde{T} * {}_0\mathcal{Y}^\dagger \bar{S} = \frac{1}{2} \bar{T}^\dagger * {}_2\mathcal{Y} * \tilde{T} * {}_0\mathcal{Y}^\dagger \bar{S} \quad (3.8)$$

$$= \bar{O}^{-1} * \bar{S} \quad (3.9)$$

We do not provide the explicit calculations here, since the derivation is nearly identical to that discussed in the previous section. The inverse operator is given by the following expression,

$$\bar{O}^{-1} = - \begin{bmatrix} \mathcal{M}_r & -\mathcal{M}_i \\ \mathcal{M}_i & \mathcal{M}_r \end{bmatrix}_{2N_{\text{pix}} \times 2N_{\text{pix}}} = -f(\beta_{ij}, \ell_{\min}, \ell_{\max}) \begin{bmatrix} \cos(2\alpha_{ij}) & -\sin(2\alpha_{ij}) \\ \sin(2\alpha_{ij}) & \cos(2\alpha_{ij}) \end{bmatrix}. \quad (3.10)$$

Note that the kernel is different by a mere change in sign on the off-diagonals of the block matrix as compared to Eq. (3.5). We can evaluate the Stokes Q & U parameters from the scalar E & B fields by evaluating the following expression,

$$\begin{bmatrix} Q_i \\ U_i \end{bmatrix} = -\Delta\Omega \sum_{j=1}^{N_{\text{pix}}} f(\beta_{ij}, \ell_{\min}, \ell_{\max}) \begin{bmatrix} \cos(2\alpha_{ij}) & -\sin(2\alpha_{ij}) \\ \sin(2\alpha_{ij}) & \cos(2\alpha_{ij}) \end{bmatrix} \begin{bmatrix} E_j \\ B_j \end{bmatrix}, \quad (3.11)$$

where all the symbols have their usual meaning. The above equation can again be expressed more concisely as follows,

$$[Q + iU](\hat{n}_0) = -\Delta\Omega \sum_{j=1}^{N_{\text{pix}}} \left( \sum_{\ell=\ell_{\min}}^{\ell_{\max}} \frac{2\ell+1}{4\pi} \sqrt{\frac{(\ell-2)!}{(\ell+2)!}} P_\ell^2(\beta_{0j}) \right) \left( e^{i2\alpha_{0j}} [\mathbf{E} + i\mathbf{B}] (\hat{\mathbf{n}}_j) \right) \quad (3.12a)$$

$${}_{+2}X(\hat{n}_0) = - \left( \left[ \sum_{\ell=\ell_{\min}}^{\ell_{\max}} \sqrt{\frac{2\ell+1}{4\pi}} Y_{\ell 2} \right] \circ [E + iB] \right) = - \left\{ \mathcal{M} \circ [E + iB] \right\}(\hat{n}_0) \quad (3.12b)$$

which is to be interpreted in the same manner as Eq. (3.7). Note that the only change in the convolution kernel as compared to that in Eq. (3.5) is that the signs of the off-diagonal block matrices are reversed. Alternatively, the  $Y_{\ell 2}$  functions are not conjugated. This can again be simply understood as constructing a spin-2 field by taking a product of a spin-0 field:  $[E + iB]$  with a spin +2 field:  $\exp(+i2\alpha)$ . The radial dependence of the operator  $\bar{O}^{-1}$  is identical to the that of  $\bar{O}$  as one may have expected. In this case all the coordinate dependence is encoded in the function  $\exp(+i2\alpha)$ , which is ill-defined at the poles ( $\beta \rightarrow 0, \pi$ ) and hence the radial functions have to vanish at these locations, which is the case for the same reasons discussed previously.

### 3.3 Decomposing Q & U Stokes parameters into those corresponding to E & B modes respectively

The Stokes Q & U parameters can be decomposed into the scalar modes E & B and vice versa, as seen in the previous sections. The E & B modes are orthogonal to each other, in the sense that their respective operators are orthogonal to each other as seen in Eq. (2.12b). It is possible to decompose the Stokes vector  $\bar{P}$  into one  $\bar{P}_E$  that purely contributes to E modes and another  $\bar{P}_B$  that purely contribute to the B modes of polarization. We can only measure the total Stokes vector which is a sum of the Stokes vectors corresponding to the respective scalar modes. In this section we derive the real space operators which directly perform this decomposition, without ever having to evaluate the E & B modes. The derivation is similar to that discussed in Sec. 3.1, though the algebra is a little more involved in this case. Here we use the harmonic space projection operators  $\tilde{O}_{E/B}$ , defined in Eq. (2.11), to derive the respective real space operators. The Stokes parameters corresponding to each scalar mode are given by the following expressions,

$$\bar{P}_E = [\bar{T}^{-1} * {}_2\mathcal{Y} * \tilde{T} * \tilde{O}_E * \tilde{T}^{-1} * {}_2\mathcal{Y}^\dagger * \bar{T}] * \bar{P}, \quad (3.13)$$

$$= \left[ \frac{1}{4} \bar{T}^\dagger * {}_2\mathcal{Y} * \tilde{T} * \tilde{O}_E * \tilde{T}^\dagger * {}_2\mathcal{Y}^\dagger * \bar{T} \right] * \bar{P},$$

$$= \bar{O}_E * \bar{P},$$

$$\bar{P}_B = [\bar{T}^{-1} * {}_2\mathcal{Y} * \tilde{T} * \tilde{O}_B * \tilde{T}^{-1} * {}_2\mathcal{Y}^\dagger * \bar{T}] * \bar{P}, \quad (3.14)$$

$$= \left[ \frac{1}{4} \bar{T}^\dagger * {}_2\mathcal{Y} * \tilde{T} * \tilde{O}_B * \tilde{T}^\dagger * {}_2\mathcal{Y}^\dagger * \bar{T} \right] * \bar{P},$$

$$= \bar{O}_B * \bar{P}.$$

We contract over all the matrix operators to arrive at the the real space operators. On working through the algebra it can be shown that the real space operators have the following form,

$$\bar{O}_{E/B} = 0.5 \begin{bmatrix} \mathcal{I}_r & \mathcal{I}_i \\ -\mathcal{I}_i & \mathcal{I}_r \end{bmatrix} \pm \begin{bmatrix} \mathcal{D}_r & \mathcal{D}_i \\ \mathcal{D}_i & -\mathcal{D}_r \end{bmatrix}, \quad (3.15)$$

where  $\mathcal{I}_r$  &  $\mathcal{D}_r$  and  $\mathcal{I}_i$  &  $\mathcal{D}_i$  are the real and complex parts of the following complex functions,

$$\mathcal{I} = \mathcal{I}_r + i\mathcal{I}_i = \sum_{\ell m} {}_{-2}Y_{\ell m}(\hat{n}_i) {}_{-2}Y_{\ell m}^*(\hat{n}_j),$$

$$\mathcal{D} = \mathcal{D}_r + i\mathcal{D}_i = \sum_{\ell m} {}_2Y_{\ell m}(\hat{n}_i) {}_2Y_{\ell m}^*(\hat{n}_j).$$

These functions can be further simplified using the properties of spin spherical harmonics listed in Appendix 6.1. Specifically it can be shown that these functions reduce to the following mathematical forms,

$$\mathcal{I}(\hat{n}_i, \hat{n}_j) = \sum_{\ell} \sqrt{\frac{2\ell+1}{4\pi}} {}_{-2}Y_{\ell 2}(\beta_{ij}, \alpha_{ij}) e^{i2\gamma_{ij}} = \mathcal{I}_r + i\mathcal{I}_i, \quad (3.16a)$$

$$\mathcal{I}_r + i\mathcal{I}_i = \left[ \cos(2\alpha_{ij} + 2\gamma_{ij}) + i \sin(2\alpha_{ij} + 2\gamma_{ij}) \right] {}_{-2}f(\beta_{ij}, \ell_{\min}, \ell_{\max}), \quad (3.16b)$$

$$\mathcal{D}(\hat{n}_i, \hat{n}_j) = \sum_{\ell} \sqrt{\frac{2\ell+1}{4\pi}} {}_2Y_{\ell 2}(\beta_{ij}, \alpha_{ij}) e^{-i2\gamma_{ij}} = \mathcal{D}_r + i\mathcal{D}_i, \quad (3.17a)$$

$$\mathcal{D}_r + i\mathcal{D}_i = \left[ \cos(2\alpha_{ij} - 2\gamma_{ij}) + i \sin(2\alpha_{ij} - 2\gamma_{ij}) \right] {}_{+2}f(\beta_{ij}, \ell_{\min}, \ell_{\max}), \quad (3.17b)$$

where the functions,

$${}_{\pm 2}f(\beta, \ell_{\min}, \ell_{\max}) = \sum_{\ell=\ell_{\min}}^{\ell_{\max}} \sqrt{\frac{2\ell+1}{4\pi}} {}_{\pm 2}f_{\ell}(\beta), \quad (3.18)$$

can be expressed in terms of  $P_{\ell}^2$  Legendre polynomials and are given by the following explicit mathematical forms,

$$\begin{aligned} {}_{\pm 2}f_{\ell}(\beta) = 2 \frac{(\ell-2)!}{(\ell+2)!} \sqrt{\frac{2\ell+1}{4\pi}} & \left[ -P_{\ell}^2(\cos \beta) \left( \frac{\ell-4}{\sin^2 \beta} + \frac{1}{2}\ell(\ell-1) \pm \frac{2(\ell-1)\cos \beta}{\sin^2 \beta} \right) \right. \\ & \left. + P_{\ell-1}^2(\cos \beta) \left( (\ell+2) \frac{\cos \beta}{\sin^2 \beta} \pm \frac{2(\ell+2)}{\sin^2 \beta} \right) \right]. \end{aligned} \quad (3.19)$$

Finally, the Stokes parameters corresponding to the respective scalar fields are given by evaluating the following expressions,

$$\begin{aligned} \begin{bmatrix} Q_i \\ U_i \end{bmatrix}_{E/B} &= \sum_{j=1}^{N_{\text{pix}}} \left\{ {}_{-2}f(\beta_{ij}, \ell_{\min}, \ell_{\max}) \begin{bmatrix} \cos(2\alpha_{ij} + 2\gamma_{ij}) & \sin(2\alpha_{ij} + 2\gamma_{ij}) \\ -\sin(2\alpha_{ij} + 2\gamma_{ij}) & \cos(2\alpha_{ij} + 2\gamma_{ij}) \end{bmatrix} \begin{bmatrix} Q_j \\ U_j \end{bmatrix} \right. \\ & \left. \pm {}_{+2}f(\beta_{ij}, \ell_{\min}, \ell_{\max}) \begin{bmatrix} \cos(2\alpha_{ij} - 2\gamma_{ij}) & \sin(2\alpha_{ij} - 2\gamma_{ij}) \\ \sin(2\alpha_{ij} - 2\gamma_{ij}) & -\cos(2\alpha_{ij} - 2\gamma_{ij}) \end{bmatrix} \begin{bmatrix} Q_j \\ U_j \end{bmatrix} \right\} 0.5\Delta\Omega, \end{aligned} \quad (3.20)$$

where all the symbols have their usual meaning. The above expression can be cast in the following simplified form,

$${}_{+2}X_{E/B} = 0.5\Delta\Omega \sum_{j=1}^{N_{\text{pix}}} {}_{-2}f(\beta_{ij}) e^{-i2(\alpha_{ij} + \gamma_{ij})} {}_{+2}X_j \pm {}_{+2}f(\beta_{ij}) e^{i2(\alpha_{ij} - \gamma_{ij})} {}_{+2}X_j^*, \quad (3.21a)$$

$$= 0.5 \left\{ \mathcal{I}^* \circ {}_{+2}X \pm \mathcal{D} \circ {}_{+2}X^* \right\}, \quad (3.21b)$$

where in Eq. (3.21a) we have suppressed the explicit multipole dependence of functions  $\pm_2 f$  for brevity and in Eq. (3.21b)  $\circ$  denotes a convolution.

It is easy to show that the operator  $\mathcal{D}$  is a complex but symmetric matrix and that the operator  $\mathcal{I}$  is Hermitian. The function  $I$  is a band limited version of the delta function ( $\lim_{\ell \rightarrow \infty} \mathcal{I} = \delta(\hat{n}_i - \hat{n}_j)$ ), when interpreted as a matrix operator forms a band limited version of the identity matrix. Though its non-local ( $\mathcal{I} \neq 0$  when  $\hat{n}_i \neq \hat{n}_j$ ) owing to the band limit, for all practical purposes the operator  $\mathcal{I}$  acts like an identity operator as is confirmed by the following identities it satisfies: (i)  $\mathcal{I} * \mathcal{I} = \mathcal{I}$ ; (ii)  $\mathcal{D} * \mathcal{I} = \mathcal{D}$ . Also  $\mathcal{D}^*$  is the inverse of  $\mathcal{D}$  in this band limited sense:  $\mathcal{D}^* * \mathcal{D} = I$ . Using these properties of the operators  $\mathcal{I}$  and  $\mathcal{D}$ , one can verify that the real space operators satisfy the following identities,

$$\bar{O}_E * \bar{O}_E = \bar{O}_E ; \quad \bar{O}_B * \bar{O}_B = \bar{O}_B , \quad (3.22a)$$

$$\bar{O}_E * \bar{O}_B = 0 , \quad (3.22b)$$

$$\bar{O}_E + \bar{O}_B = \mathcal{I} , \quad (3.22c)$$

which are the real space analogues of Eq. (2.12). While testing the above stated identities one encounters terms like  $\mathcal{D} * \mathcal{I}^*$ ,  $\mathcal{I}^* * \mathcal{I}$  and  $\mathcal{I} * \mathcal{I}^*$  which cannot be simply interpreted, but they always occur in pairs with opposite signs, hence exactly canceling each other. Note that unlike in the harmonic case, the sum of the operators is not exactly an identity matrix.  $\Rightarrow$  Isn't it possible to do some real space operations which doesn't care for the band limit but still returns the required decomposition into the respective scalar modes? This indicates the loss of information occurred from the original data due to making this transformations with some assumed band limit. If one forces the sum of the operators to be exactly an identity operator, then one compromises on the orthogonality property of the  $\bar{O}_E$  &  $\bar{O}_B$  operators.

### 3.4 Visualizing the convolution kernels

*Evaluating the local kernels:* Let us consider the case when one of the coordinates coincides with the north pole (more formally this refers to the point  $\theta_0 \rightarrow 0$  while moving along the longitude  $\phi_0 = 0$ ), say  $\hat{n}_0 = (\theta_0, \phi_0) = (0, 0)$ . In this case the Euler angles in the  $z - y1 - z2$  convention are simply given by:  $(\alpha, \beta, \gamma) = (\phi_i, \theta_i, 0)$ , where  $(\theta_i, \phi_i)$  denote the coordinates of the location  $\hat{n}_i$ . Since the Euler angle  $\gamma = 0$  when rotations are defined with respect to the pole, the respective kernels simplify to the following forms,

$$\mathcal{M}(\hat{n}_0, \hat{n}_i) = \sum_{\ell} \sqrt{\frac{2\ell+1}{4\pi}} Y_{\ell 2}(\theta_i, \phi_i) = \sum_{\ell} {}_0 a_{\ell 2} {}_0 Y_{\ell 2}(\theta_i, \phi_i), \quad (3.23a)$$

$$\mathcal{I}(\hat{n}_0, \hat{n}_i) = \sum_{\ell} \sqrt{\frac{2\ell+1}{4\pi}} {}_{-2} Y_{\ell 2}(\theta_i, \phi_i) = \sum_{\ell} {}_{-2} a_{\ell 2} {}_{-2} Y_{\ell 2}(\theta_i, \phi_i), \quad (3.23b)$$

$$\mathcal{D}(\hat{n}_0, \hat{n}_i) = \sum_{\ell} \sqrt{\frac{2\ell+1}{4\pi}} {}_2 Y_{\ell 2}(\theta_i, \phi_i) = \sum_{\ell} {}_2 a_{\ell 2} {}_2 Y_{\ell 2}(\theta_i, \phi_i). \quad (3.23c)$$

The kernels centered around any other location  $\hat{n}_j = (\theta_j, \phi_j)$  are simply given by evaluating the respective spherical harmonic sums using the rotated harmonic coefficients given by,

$${}_s a_{\ell m} = D_{m2}^{\ell}(\phi_j, \theta_j, 0) {}_s a_{\ell 2}, \quad (3.24)$$

where  $D_{m2}^{\ell}$  are the Wigner-D functions and  ${}_s a_{\ell 2} = \sqrt{\frac{2\ell+1}{4\pi}}$ . These rotation operations can be carried out using inbuilt Healpix routine `rotate_alm`, while the convolution kernels can be synthesized by evaluating the respective spherical harmonic sums using the `alm2map` routine.

We compute the local convolution kernels using the procedure outlined in the discussion above. Since its not easy to imagine how the Euler angles vary as a function of position of the central pixel we depict the kernels at different locations in Fig. 1, to give a sense of how these kernels vary across the sphere. For illustration these functions are sampled at a very high Healpix resolution parameter of `NSIDE=2048`. All the plots have been rotated such that the central location  $\hat{n}_j$  around which the kernels are computed lies in the centre marked by the back circle.

The real and imaginary part of the kernel  $\mathcal{M}$  are identical irrespective of changes in the galactic latitude and longitude of the central pixel. Note that these functions are not distorted when a part of the domain overlaps with the poles, as can be seen in the first three rows of Fig. 1. Both these facts can be associated with the fact that this function does not depend on the Euler angle  $\gamma$ .

The function  $\mathcal{D}$  varies significantly as a function of galactic latitude of the central pixel. It varies from having a two fold symmetry at the poles to having a four fold symmetry at the equator as seen in the middle two columns of Fig. 1. This change in behavior is primarily due to the dependence on the Euler angle  $\gamma$ . When the central pixel is nearly at the pole,  $\gamma$  vanishes, and the azimuthal part of the function  $D$  is identical to that of  $\mathcal{M}$  and hence the two function look very similar as seen in the first row of Fig. 1. Also note that this function is distorted as parts of its domain pass the galactic poles.

The function  $\mathcal{I}$  shows similar behavior, varying with latitude, having an identical azimuthal behavior near the poles and being distorted in parts that overlap with the galactic poles. **This function, in the case of an infinite band limit reduces to a delta function at the position of the central pixel ( $\lim_{\ell_{\max} \rightarrow \infty} : \mathcal{I}_r \rightarrow \delta(\hat{n}_0 - \hat{n}')$ ,  $\mathcal{I}_i \rightarrow 0$ ), as discussed previously.**

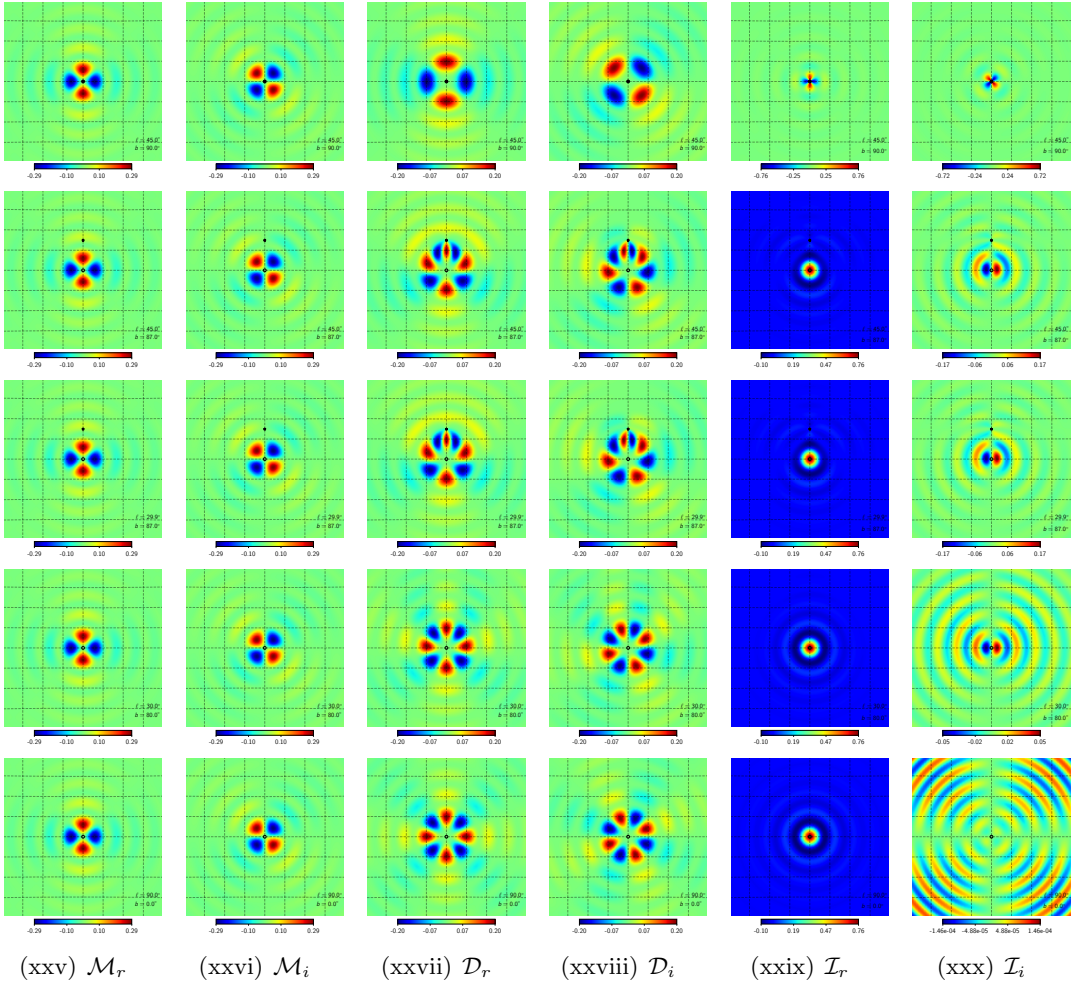


**Figure 1.** This panel of figure depicts the various parts of the convolution kernel, discussed in Sec. 3. These kernels have been evaluated with the band limit:  $\ell \in [2, 192]$ . The functions have been sampled at an NSIDE=2048 resolution for visual appeal. The size of each panel is approximately  $16^\circ \times 16^\circ$  and the grid lines are marked at 2 degree separations. The black circles denotes the position of the central pixel around which the convolution kernels have been evaluated. The black star marks the location of the north galactic pole. The five rows depict the kernels at different location on the sphere and the galactic coordinates of the central pixel are specified in each panel.

Hints of this behavior can be seen by comparing the amplitudes of the real and imaginary parts of this function near the equator, depicted in the fifth row of the last two columns of Fig. 1. However note that this function significantly deviates from this behavior at higher galactic latitudes. The real and imaginary parts of this function contribute nearly equally near the vicinity of the poles. We invariably work with a specific band limit, hence both the real and imaginary parts of this functions make important non-zero contributions.

We reiterate that all the function are invariant under changes in longitude of the central pixel, the latitude being held fixed as can be seen by comparing the figures in the second row (evaluated at  $[b, \ell] = [87^\circ, 45^\circ]$ ) and third row (evaluated at  $[b, \ell] = [87^\circ, 30^\circ]$ ) of Fig. 1, as one may have expected.

### 3.5 Quantifying the non-locality of E & B modes

As seen in the previous sections, all the kernels separate into a part which depends only on the angular distance between pixels and another part that depends on the azimuthal orientation around the central pixel. The radial part of the kernels determines the non-locality of the operator. We numerically compute the radial kernels:  $f_{,+2}f$  &  $-_2f$  by evaluating the respective multipole sums given in Eq. (3.4b) and Eq. (3.18) in the band limit  $\ell \in [= 2, 192]$ . The resultant functions are depicted in Fig. 2. Note that the function  $f(\beta)$ , which forms

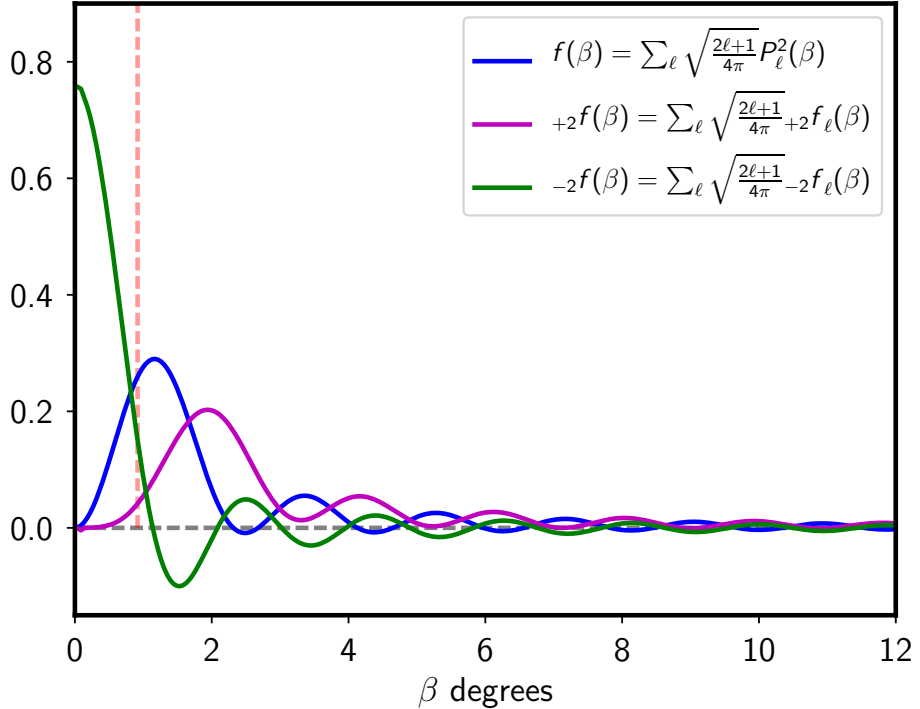


**Figure 2.** The figure depicts the radial part of the convolution kernels. These radial function have been evaluated with the band limit fixed at  $\ell \in [2, 192]$ . The vertical dashed line marks the approximate size of a NSIDE=64 Healpix pixel.

the radial part of the real space convolution kernel that translates the Stokes parameters Q & U to scalars E & B, has a vanishing contribution from the location of the central pixel ( $\beta \rightarrow 0$ ). Recall that the fields E & B are scalar and hence expected to be immune to coordinate definitions. The locally defined Stokes parameters however necessarily depend on the coordinate definition. Therefore, this nature of the radial kernel is to be expected in order for it to satisfy the requirement of the derived quantities being coordinate independent.

The functions  $+_2f(\beta)$  &  $-_2f(\beta)$ , both contribute to the convolution kernels which decompose the Stokes parameters into those corresponding to the respective scalar modes E & B.  $-_2f(\beta)$  form the radial part of the band limited delta function  $I$  and hence it contributes the most at the location of the central pixel.  $+_2f(\beta)$  again has a vanishing contribution near the central pixel and it dominantly contributes in the neighbouring regions which are approximately at least 1 pixel distance away from the central pixel.

It is clear from previous discussions that that the non-locality of the E and B modes is determined by the radial part of the convolution kernels. To quantify this non-locality as

a function of the maximum multipole accessible for analysis, we evaluate the radial part of the convolution kernel for different values of  $\ell_{\max}$ , while keeping the lowest multipole fixed at  $\ell_{\min} = 2$ . The set of radial kernels so derived are plotted in Fig. 3. All the function have been normalized such that their global maxima is set to unity. Note that on increasing  $\ell_{\max}$  the radial kernels shift to the left, attaining fractions of their global maxima at progressively small angular distances  $\beta$  from the central pixel.

We have observed that the radial functions derived by evaluating the multipole sums to different maximum multipoles are self similar. Specifically these functions follow an interesting telescoping and scaling property:

$$rf(\beta, 2, \ell_{\max}) \approx \left[ \frac{\ell_{\max}}{\ell'_{\max}} \right]^2 rf(\beta' = \frac{\ell_{\max}}{\ell'_{\max}} \beta, 2, \ell'_{\max}),$$

where  $rf$  denotes all the different radial functions. We can understand the shifting left of the radial kernels on increasing the maximum multipole using this property. Lets say the function  $rf(\beta, \ell'_{\max})$  transition to being monotonously below some fraction of the global maxima at an angular distance of  $\beta_0$ . The function  $rf(\beta', \ell_{\max})$ , given  $\ell_{\max} > \ell'_{\max}$ , reaches the same transition point  $\beta' = \beta_0$  at a smaller value of  $\beta$  owing to the fact that  $\ell_{\max}/\ell'_{\max}$  is greater than unity. The amplitude scaling of the functions is irrelevant since the transition point is always described in terms of the fraction of the global maxima of the function.

We are primarily interested in the non-local dependence of the scalar modes E & B on the Stokes parameters Q & U. We define the value of the abscissa at which the function  $f(\beta, \ell_{\min}, \ell_{\max})$  transits to being monotonously below 1% of the maxima of the function as the non-locality parameter:  $\beta_o$ . For a  $\ell_{\max} = 24$ , the maximum multipole accessible on a Nside=8 Healpix map, the non-locality parameter  $\beta_0 = 180^\circ$ , since the radial function never falls monotonously below 1% of the global maxima of the function. Using the self similar property of the radial function discussed above, we define the following:  $\beta_o = \min(180, 180 \frac{24}{\ell_{\max}})$  as the non-locality parameter, given the maximum multipole  $\ell_{\max}$ .  $\beta_0$  is not very sensitive to  $\ell_{\min}$ , though it can be important on making drastic changes to  $\ell_{\min}$ .  $\Rightarrow$  Quantify how changing  $\ell_{\min}$  changes  $\beta_0$

The envelope of the radial kernel  $f(\beta, \ell_{\min}, \ell_{\max})$  is observed to have a power law relation to the angular distance  $\beta$  as seen in Fig. 3. At small values of  $\beta$ , which corresponds to the flat sky limit, the radial function is proportional to  $\beta^2$ . In the intermediate range, a fit by eye indicates that the envelope of the function is well represented by the power law  $\beta^{-1.5}$ .  $\Rightarrow$  There isn't too much of a discussion surrounding the function  $\pm f(\beta)$ .

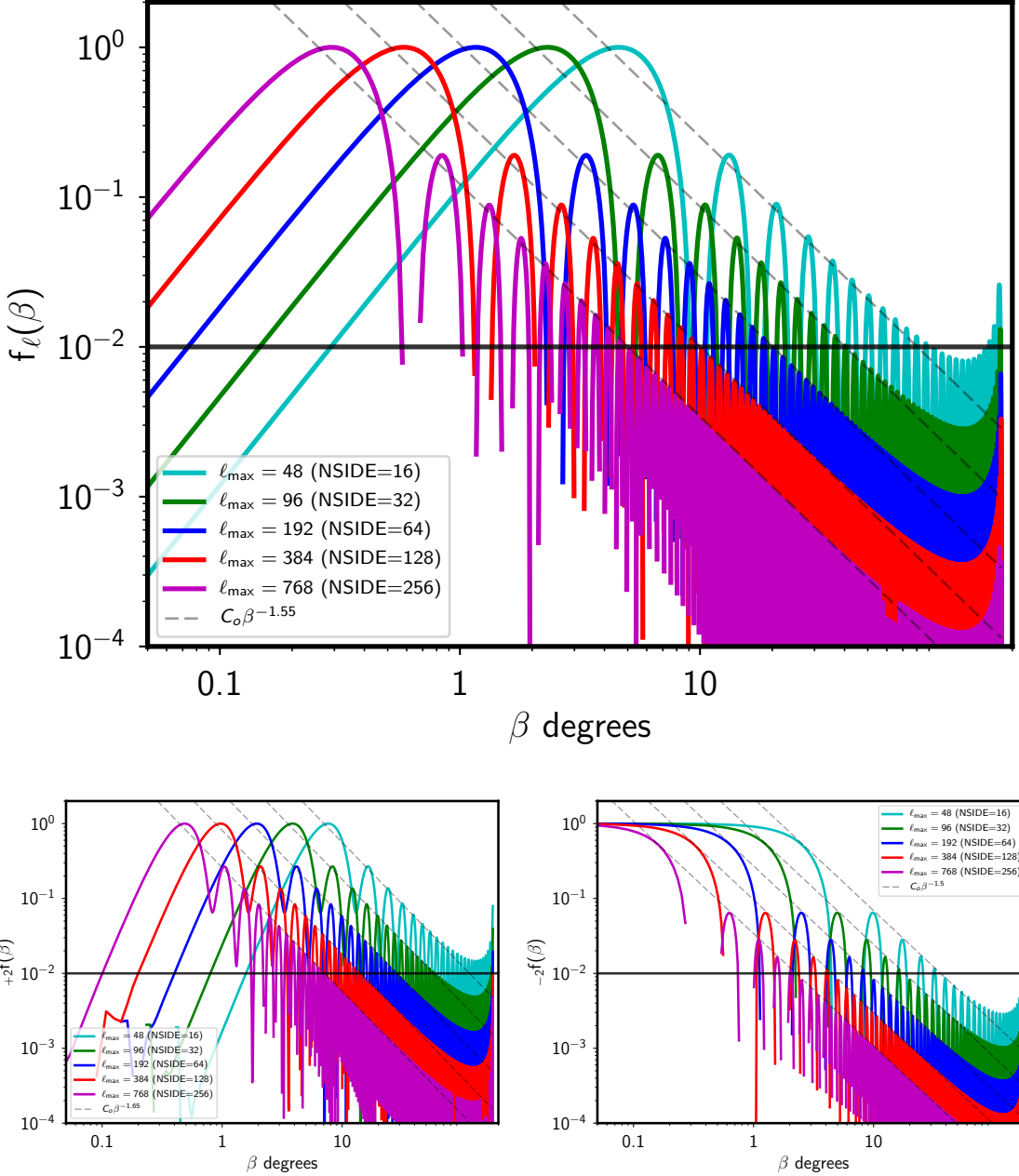


**Figure 3.** The top panel shows a plot of the radial kernels  $f(\beta, \ell_{\min}, \ell_{\max})$  while the bottom left and right panels show the radial functions  ${}_{+2}f(\beta, \ell_{\min}, \ell_{\max})$  &  ${}_{-2}f(\beta, \ell_{\min}, \ell_{\max})$  respectively, for different  $\ell_{\max}$  as indicated by the legends and fixed  $\ell_{\min} = 2$ . The curves for each of these functions have been normalized such that the maximum of the curve is set to unity. The horizontal solid black line marks the location where the amplitude of the kernel falls below 1% of its maximum. The slanted dashed black lines indicate a power law fit (by eye) to the envelope of the radial functions. While the envelopes for function  $f(\beta)$  &  ${}_{-2}f(\beta)$  are fit well by the power law  $\propto \beta^{-1.5}$ , the envelope for the function  ${}_{+2}f(\beta)$  is seen to have a slightly steeper fall off  $\propto \beta^{-1.65}$ .

⇒ How does the radial kernel reduce to unity on evaluating the the operator on to its inverse ? This will be important to understand how to define alternate radial functions.

## 4 Generalized operators

The azimuthal dependence of the convolution kernels which translate the Stokes parameters Q & U to the scalar E & B is determined by the spin properties of the field being operated upon and the spin of the resultant fields. Hence there is no freedom in the choice of function for the azimuthal dependence of the convolution kernels. The radial part of the function however is determined by the choice of the basis functions. It is possible to generalize these convolution kernels by choosing alternate forms for the radial functions.

We can characterize different forms of the radial kernel by introducing the following harmonic space operator,

$$\tilde{\mathcal{G}} = \begin{bmatrix} g_\ell^E & 0 \\ 0 & g_\ell^B \end{bmatrix}, \quad (4.1)$$

where the functions  $g_\ell^E$  and  $g_\ell^B$  represent the harmonic representation of the modified radial functions and can in the most general case be chosen to be different for E and B modes. To simplify the discussion and without loosing this generality we proceed with the assumption  $g_\ell^E = g_\ell^B = g_\ell$ . We can chose this function to be any arbitrary function and it will allow us to define some convolution operator which either translates Stokes Q & U parameters to scalars E & B or vice versa. Given  $\tilde{\mathcal{G}}$  the modified forward and inverse convolution kernels are given by the following expressions,

$$\bar{O}' = {}_0\mathcal{Y} * \tilde{T}^{-1} * \tilde{\mathcal{G}} * {}_2\mathcal{Y}^\dagger * \bar{T}, \quad (4.2a)$$

$$\bar{O}'^{-1} = \bar{T}^{-1} * {}_2\mathcal{Y} * \tilde{\mathcal{G}}^{-1} * \tilde{T} * {}_0\mathcal{Y}^\dagger \quad (4.2b)$$

where we have used the primed notation to distinguish these generalized operators from the default operators defined in Sec. 3.1 and Sec. 3.2. Note that for an arbitrary choice of  $\tilde{\mathcal{G}}$  only one of the operators in Eq. (4.2) is well defined, since  $\tilde{\mathcal{G}}^{-1}$  may be ill defined. If we require both the forward and inverse hold true, then we are constrained in choosing  $\tilde{\mathcal{G}}$  such that its inverse is well defined.

The radial part of these generalized convolution kernels is now given by the following expressions,

$$G_{QU \rightarrow EB}(\beta) = G(\beta) = \sum_{\ell=2}^{\ell_{\max}} g_\ell \frac{2\ell+1}{4\pi} \sqrt{\frac{(\ell-2)!}{(\ell+2)!}} P_\ell^2(\cos \beta) \quad (4.3a)$$

$$G_{EB \rightarrow QU}(\beta) = G^{-1}(\beta) = \sum_{\ell=2}^{\ell_{\max}} g_\ell^{-1} \frac{2\ell+1}{4\pi} \sqrt{\frac{(\ell-2)!}{(\ell+2)!}} P_\ell^2(\cos \beta), \quad (4.3b)$$

where  $g_\ell$  are the same multipole function as those appearing in  $\tilde{\mathcal{G}}$ . If one chooses different forms of  $g_\ell$  for E and B modes then the radial function are defined accordingly. Given this general definition for the radial function  $G(\beta)$ , note that the default radial function  $f(\beta)$  is just a special case resulting from the choice  $\tilde{\mathcal{G}} = \tilde{\mathcal{I}}$  ( $g_\ell = 1$ ). Note that for this choice of  $\tilde{\mathcal{G}}$  the inverse is trivial  $\tilde{\mathcal{G}}^{-1} = \tilde{\mathcal{G}}$  and therefore  $G^{-1}(\beta) = G(\beta)$ .

While defining these alternate operators by modifying the radial part of the kernels, it seems more natural to make a choice on the real space function  $G(\beta)$  as compared to

choosing the multipole function  $g_\ell$ . Using the orthogonality property of associated Legendre polynomials it can be shown that the multipole function  $g_\ell$  is given by the following integral over the radial function  $G(\beta)$ ,

$$g_\ell = 2\pi \sqrt{\frac{(\ell-2)!}{(\ell+2)!}} \int_0^\pi G(\beta) P_\ell^2(\cos \beta) d\cos \beta. \quad (4.4)$$

Here it is important to note that the radial function  $G(\beta)$  has to be chosen such that it vanishes at  $\beta = 0$  and  $\beta = \pi$ . One way to understand this is that the associated Legendre polynomials  $P_\ell^2 \propto \sin^2 \beta$  vanish at these values of the abscissa and hence cannot be used to describe functions which don't have this property. Another way to understand this requirements is that at these locations the coordinate dependence of the Stokes parameters cannot be integrated out, since the azimuthal angle is ill defined and hence the convolution kernel needs to have vanishing contribution from these locations. **The normalization of these functions is not critically important, since any choice defines a convention. It is important to ensure consistency with the convention once a choice has been made.**  $\Rightarrow$  find a better location for this

In contrast to the radial function  $G(\beta)$  an instrumental beam function appropriately normalized has the property  $B(\beta) \rightarrow 1$  as  $\beta \rightarrow 0$ . A circularly symmetric beam is represented in harmonic space by the multipole function  $b_\ell$  which can be derived by evaluating the coefficients of expansion of the function  $B(\beta)$  defined at the pole in the Legendre polynomial  $P_\ell^0$  basis. The effective instrument beam is almost always identical for  $E$  and  $B$  modes.  $\Rightarrow$  Distinguishing E/B localization characterized by  $g_\ell$  from E/B smoothing characterized by  $b_\ell$ .

$$B(\beta) = \sum_{\ell=0}^{\ell_{\max}} \frac{2\ell+1}{4\pi} b_\ell P_\ell^0(\cos \beta), \quad (4.5)$$

$\Rightarrow$  A co-polarized beam which measures the Stokes parameters is not the same as a smoothing beam measuring a scalar field. Is it important to discuss the polarization beam details here? Though the real space behavior of these two function  $G(\beta)$  and  $B(\beta)$  has important differences, in harmonic space they play identical roles. Therefore it is possible to interpret the beam harmonic coefficients as those representing some modified radial kernel. The modified radial kernel resulting from a few example Gaussian beams are depicted in Fig. 4(i). it is possible to interpret the harmonic representation  $g_\ell$  of the radial function  $G(\beta)$  as those corresponding to some circularly symmetric instrument beam function. The beam function corresponding to the default radial kernel and the modified radial kernel  $G(\beta)$  are depicted in Fig. 4(iii).

$\Rightarrow$  Move the following two paragraphs to final discuss The discussion till now gives the impression that using the localized convolution kernels is no different from using the default kernel and altering the spherical harmonic coefficients of expansion of the relevant fields by appropriately operating on them with the effective beam functions  $g_\ell$ . To appreciate the difference between these two, it is important to realize that in general one can make a choice of a radial function which may not have a band limited description. In such a case these two method of evaluating the relevant fields is not identical. An example of this claim is depicted in Fig. 4.

Another important thing to realize is that the harmonic coefficients derived from default full sky operations get some contributions from different portions of sky. For instance evaluating

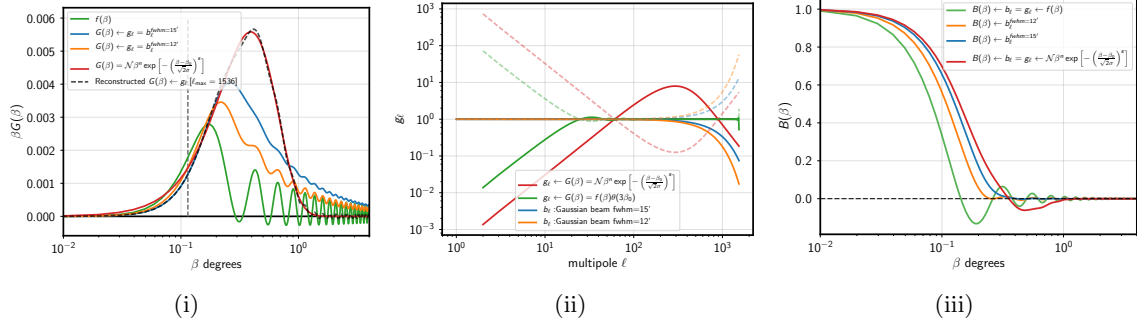


**Figure 4.** *Left:* The vertical dashed gray line depicts the approximate pixel size  $\Delta_{\text{pix}} = \sqrt{\frac{4\pi}{N_{\text{pix}}}}$  of a  $N_{\text{side}}=512$  Healpix map. The green line depicts the default radial kernel  $f(\beta)$  defined in Eq. (3.4). The blue and orange lines depict the modified radial function resulting the beam harmonics  $b_\ell$  corresponding to Gaussian beams with  $\text{fwhm}=15$  & 12 arcminutes respectively. The red curve depicts an example modified radial function:  $G(\beta) = \mathcal{N}\beta^n \exp\left[-\left(\frac{\beta-\beta_0}{\sqrt{2}\sigma}\right)^s\right]$  with parameters set to the following values [ $n = 1$ ;  $\beta_0 = 0$ ;  $\sigma = 2\Delta_{\text{pix}}$ ;  $s = 1.5$ ]. The black dashed curve depicts the band limited reconstruction of the modified radial function  $G(\beta)$ . We intentionally have plotted  $\beta G(\beta)$  to clearly depict the high  $\beta$  behavior of these functions. *Middle:* This figure depicts the harmonic representation of the respective radial functions as indicated by the legend. The dashed curves of the corresponding color depict the inverse of the harmonic functions. *Right:* This figure depicts the beam function  $B(\beta)$  evaluated from interpreting the respective harmonic functions as those corresponding to an instrument beam.

the E and B fields in the vicinity of the poles are prone to receiving significant contributions from strong foregrounds near the equator. Correcting the harmonic coefficients of expansion with the effective beam function does not cancel these non-local contribution. On the contrary by performing the convolution with the localized real space kernels, the regions which contribute to the local field evaluations are predetermined by the choice of the radial function.

#### 4.1 Recovering the default E and B mode spectra

The convolution kernels defined using a modified radial function  $G(\beta)$  returns some scalar  $E'$  and  $B'$  mode maps,

$$\bar{S}' = \bar{O}' * \bar{P} \quad (4.6)$$

which are not the standard  $E$  and  $B$  modes maps. Since the harmonic representation  $g_\ell$  of the radial function  $G(\beta)$  can be simply interpreted as the harmonic coefficients of some beam, the spectra of the scalar fields  $E'$  and  $B'$  are related to the spectra of the spectra of the standard  $E$  and  $B$  fields via the following relation,

$$C_\ell^{EE, BB, EB} = C_\ell^{E'E', B'B', E'B'}/g_\ell^2. \quad (4.7a)$$

$$C_\ell^{TE,TB} = C_\ell^{TE',TB'} / g_\ell. \quad (4.7b)$$

The auto and cross spectra with the standard  $E$  and  $B$  fields can be recovered from the modified fields  $E'$  and  $B'$ . Their accurate recovery only relies on the inverse of the harmonic functions  $1/g_\ell$  being well behaved, which can be ensured by smartly choosing the radial function  $G(\beta)$ .

Unlike the instrument beam, the radial function  $G(\beta)$  is an analysis choice. functions are perfectly known. Since the radial kernel is perfectly known it is in principle possible to perfectly deconvolve the same. In contrast the beam function  $B\beta$  has to be inferred from measurement of point source and hence is not known exactly and therefore the deconvolution is only approximate. Even though the  $G(\beta)$  maybe such that it doesn't have an accurate band limited description, the spectra are always evaluated to a definite band limit.

## 5 Discussion

- Many CMB experiments cannot access the large angle modes due to limited sky coverage. Often the large angle analysis is deal with in pixel space owing to the non-Gaussianity of the likelihood functions. With all these as motivations we study how the radial filters are modified by removing the large scale modes. We try to understand how removing large scale modes effects the locality of the E and B map estimators. We demonstrate that it is possible to get filtered maps by using the modifying the radial filter.
- We have derived the real space kernels for translating Stokes parameters Q & U to scalars E & B and vice versa. We have also derived real space kernels which allow for direct separation of Stokes Q & U parameters without having to first evaluate the scalar field E & B.
- These kernels quantify the non-locality of the E and B fields. We have introduced the non-locality parameter  $\beta_0$  which provides a quantitative measure of the non-locality of these fields.
- Studying these real space kernels reveals that its the radial part of the kernel which knows about the band limit of the experiment. Motivation for defining radially compact kernels. We have demonstrated that using the radially compact kernels does not bias the spectral information on intermediate angular scales.
- Small field experiments like BICEP implement such radial cut offs due to limited survey area.
- Using in conjunction with FEBECOP [5] like schemes to directly infer E and B mode maps from raw maps.
- *Total convolution methods:* Since the convolution kernels can be thought of as effective beams for polarization maps, it may be possible to use total convolution methods to construct E and B mode maps.
- Separate Q and U maps for E and B: We have presented kernels which allow for decomposition of the total Stokes Q and U parameters to those corresponding to E and B modes. This could be potentially interesting, since one can now work with E and B modes foregrounds and their separations separately.  $\Rightarrow$  **But is there an issue with doing this in the standard method which involves going through the process of generating E and B modes ?**
- *Mask leakages* can be understood as arising from improper sine quadrupole and cosine quadrupole transforms on rings with holes in them due to masking. For the global mask (no point sources), by using a radially compact kernel with some  $\beta_0$ , the pixels which are at a angular distance  $\beta_0$  from the edges of the mask have unbiased estimates of the scalar fields E and B.
- The difference between the spectra derived from the local convolution maps and the reference spectra follow a definite pattern and maybe it possible to model this difference and correct for it. For this purpose one will have to model the two point correlation function for the E and B fields in terms of the Stokes Q and U maps.

- Poor sensitivity to large scale modes as the local estimated maps do no carry information from pixel which are further away than the radial cutoff. This should cause a compromise on spectral estimates of low multipoles, which correspond to large angular scales, much larger than radial cutoff.
- Cluster polarization will be measurable with future CMB experiments. These local estimators can be used to evaluate the local scalar modes of polarization.
- We have not addressed the E to B leakage issue in this work.

## 6 Appendix

### 6.1 Mathematical properties of spin spherical harmonics

The sum over  $m$  index of product of two spherical harmonic functions of spin  $s_1$  and  $s_2$  respectively, is given by the following expression [4],

$$\sum_m s_1 Y_{\ell m}^*(\hat{n}_i) s_2 Y_{\ell m}(\hat{n}_j) = \sqrt{\frac{2\ell+1}{4\pi}} {}_{s_2} Y_\ell^{-s_1}(\beta, \alpha) e^{-is_2\gamma}, \quad (6.1)$$

where  $\alpha$ ,  $\beta$  &  $\gamma$  correspond to the Euler angles that specify the rotation matrix which transforms the local cartesian coordinates defined at  $\hat{n}_i$  such that it aligns with the local cartesian coordinate system at  $\hat{n}_j$ .

The spin spherical harmonics satisfy the following orthogonality relations,

$$\int_s Y_{\ell m}(\hat{n}) {}_s Y_{\ell' m'}^*(\hat{n}) d\Omega = \delta_{\ell\ell'} \delta_{mm'}, \quad (6.2)$$

where  $s$  denotes the spin of the spherical harmonic coefficients. The numerical validity of Eq. (6.2) is only limited by the rate at which these functions are sampled on the sphere and hence this identity can be made arbitrarily accurate by choosing a sufficiently high sampling rate.

The spin spherical harmonic functions satisfy the following completeness relation,

$$\sum_{\ell m} s Y_{\ell m}(\hat{n}_i) {}_s Y_{\ell m}^*(\hat{n}_j) = \delta(\hat{n}_i - \hat{n}_j), \quad (6.3)$$

Note that the numerical validity of Eq. (6.4) is strictly true only when the sums over the indices  $(\ell, m)$  run to infinity. This is never true in practice, since the measured data invariable are band limited owing to the finite resolution of the experiments. Hence this relation is only approximately true and in more realistic scenario takes up the following function form,

$$\begin{aligned} \sum_{\ell=\ell_{\min}, m}^{\ell_{\max}} s_1 Y_{\ell m}^*(\hat{n}_i) s_2 Y_{\ell m}(\hat{n}_j) &\approx \delta(\hat{n}_i - \hat{n}_j), \\ \sum_{\ell=\ell_{\min}, m}^{\ell_{\max}} s_1 Y_{\ell m}^*(\hat{n}_i) s_2 Y_{\ell m}(\hat{n}_j) &= \sum_{\ell=\ell_{\min}}^{\ell_{\max}} \sqrt{\frac{2\ell+1}{4\pi}} {}_{s_2} Y_\ell^{-s_1}(\beta, \alpha) e^{-is_2\gamma}, \end{aligned} \quad (6.4)$$

where  $\alpha, \beta$  &  $\gamma$  are the Euler angles. A specific case of this function with  $(s = 2, \ell_{\min} = 2, \ell_{\max} = 96)$  is depicted in the last two columns of Fig. 1.

### 6.2 The flat sky limit

## References

- [1] M. Zaldarriaga, *The nature of the E-B decomposition of CMB polarization*, *Phys. Rev. D* **64** (jun, 2001) 103001, [[0106174](#)].
- [2] M. Kamionkowski, A. Kosowsky and A. Stebbins, *Statistics of cosmic microwave background polarization*, *Phys. Rev. D* **55** (1997) 7368–7388, [[9611125](#)].
- [3] J. N. Goldberg, A. J. Macfarlane, E. T. Newman, F. Rohrlich and E. C. G. Sudarshan, *Spin-s Spherical Harmonics and \eth*, *J. Math. Phys.* **8** (nov, 1967) 2155.
- [4] D. A. Varshalovich, A. N. Moskalev and V. K. Khersonskii, *Quantum Theory of Angular Momentum* (World Scientific). World Scientific, 1988.
- [5] S. Mitra, G. Rocha, K. M. Górski, K. M. Huffenberger, H. K. Eriksen, M. a. J. Ashdown et al., *FAST PIXEL SPACE CONVOLUTION FOR COSMIC MICROWAVE BACKGROUND SURVEYS WITH ASYMMETRIC BEAMS AND COMPLEX SCAN STRATEGIES: FEBECoP*, *Astrophys. J. Suppl. Ser.* **193** (mar, 2011) 5, [[1005.1929](#)].